ROTOR-TO-STATOR PARTIAL RUBBING AND ITS EFFECTS ON ROTOR DYNAMIC RESPONSE*

Agnes Muszynska, Wesley D. Franklin,
and Robert D. Hayashida
Bentley Rotor Dynamics Research Corporation
Minden, Nevada 89423, U.S.A.

This paper presents results from experimental and analytical studies on rotor–to–stationary element partial rubbings at several locations and their effects on rotor dynamic responses. The mathematical model of a rubbing rotor is given. The computer program provides numerical results which agree with experimentally obtained rotor responses.

INTRODUCTION

Rotor–to–stationary element rubbing is a serious malfunction in rotating machines. It may lead to a catastrophic failure of the machine. The rub phenomena have been recognized for a long time; literature on this subject is, however, relatively scarce and incoherent [1]. This is probably due to the fact that rotor–to–stationary element rub–related phenomena are very complex, involving several physical mechanisms, thus they represent a wide spectrum of rotating machinery dynamic problems. These problems are illustrated in Figures 1 to 4 [2].

Partial rub phenomena occurring at several radial and axial locations of the rotor are discussed in this paper. The results calculated using a mathematical model show good agreement with the experimental data.

MATHEMATICAL MODEL

Using the modal concept, a laterally symmetric (isotropic) rotor bearing/seal system is mathematically modeled for its first three lateral modes. In addition to the three modal mass lateral displacements necessary for the model, the displacements of four other axial locations at which rub can occur are included in the model. Since rub usually occurs at seal locations, the flow–related forces are introduced at these locations in addition to the system stiffness modifications, normal and friction forces, and impact losses generated by the rub. The schematic model is presented in Figure 5. The system is composed of the rotor's modal masses (M_1,M_2,M_3), stiffnesses (K_1,...,K_7), and dampings (D_1,D_2,D_3), bearing/seal's stiffnesses (K_{B1},...,K_{B4}), radial dampings (D_1,...,D_4), and fluid average circumferential velocity ratios (λ_1,...,λ_4), and the rub parameters such as radial clearances (C_1,...,C_4), coefficients of friction (μ_1,...,μ_4), restitution coefficients (κ_1,...,κ_4), and stator stiffnesses (K_{r1},...,K_{r4}). The modal parameters may be obtained from numerical analysis (using transfer matrix or finite element methods followed by reduction to three modes), and/or identified experimentally using perturbation techniques. The force equilibrium equations for the system are as follows:

*This work was partly supported by NASA George C. Marshall Space Flight Center under Contract NAS8-36719.

$$M_i\ddot{z}_i + D_{si}\dot{z}_i + K_{2i-1}(z_i-\tilde{z}_i) + K_{2i}(z_i-\tilde{z}_{i+1}) = F_{ui}e^{j(\Omega t+\varepsilon_i)} + F_{pi}e^{j\gamma}\,, \tag{1}$$

$$D_\nu\dot{\tilde{z}}_\nu/\kappa_\nu + \tilde{z}_\nu(K_{B\nu}-jD_\nu\lambda_\nu\Omega) + K_{2\nu-2}\left[\tilde{z}_\nu-z_{\nu-1}\right] + K_{2\nu-1}\left[\tilde{z}_\nu-z_\nu\right] +$$

$$+ f_\nu\left[K_{r\nu}(|\tilde{z}_\nu|-C_\nu)(1+j\mu_\nu)\right]e^{j\delta_\nu} = 0\,, \tag{2}$$

$$z_i = x_i + jy_i, \quad \tilde{z}_\nu = \tilde{x}_\nu + j\tilde{y}_\nu\,, \quad i=1,2,3\,, \quad \nu=1,2,3,4\,, \quad K_0=0\,, \quad z_4=0\,,$$

where Ω is rotative speed, $F_{ui}e^{j(\Omega t+\varepsilon_i)}$ is the mass unbalance force, $F_{pi}e^{j\gamma_i}$ the static radial preload force, f_ν the contact factor, and δ_ν the rub angular location (Fig. 6). When the contact occurs, ($|\tilde{z}_\nu| \geq C_\nu$) then $f_\nu=1$ and κ_ν = defined restitution parameter value, otherwise $f_\nu=0$ and $\kappa_\nu=1$. The rub forces are modeled in Eq. (2) by the terms $f_\nu\left[K_{r\nu}(|\tilde{z}_\nu|-C_\nu)(1+ju_\nu)\right]e^{j\delta_\nu}$ and

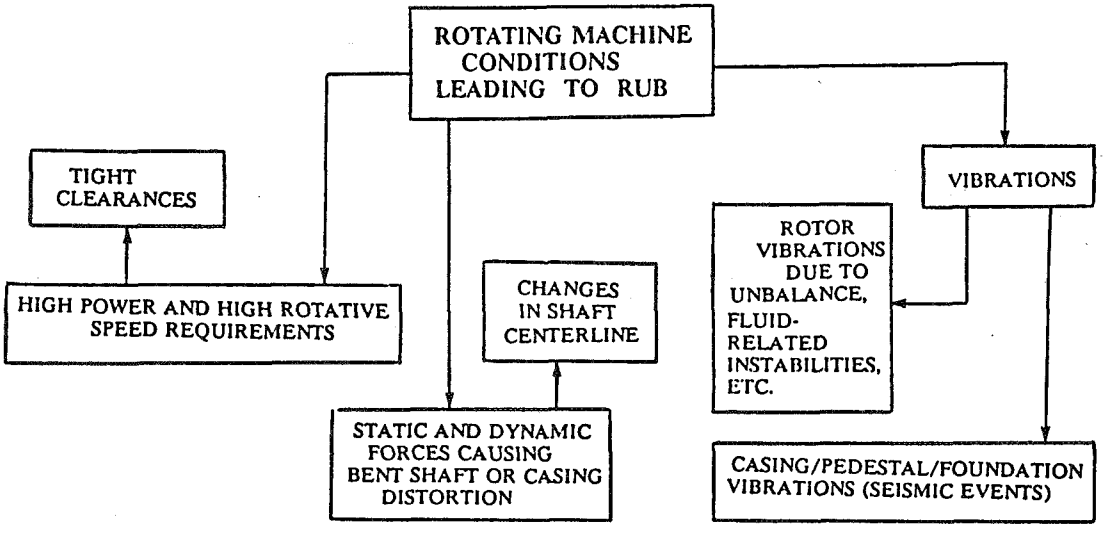

Figure 1. – Rotating machine conditions leading to rotor–to–stationary element rubbing.

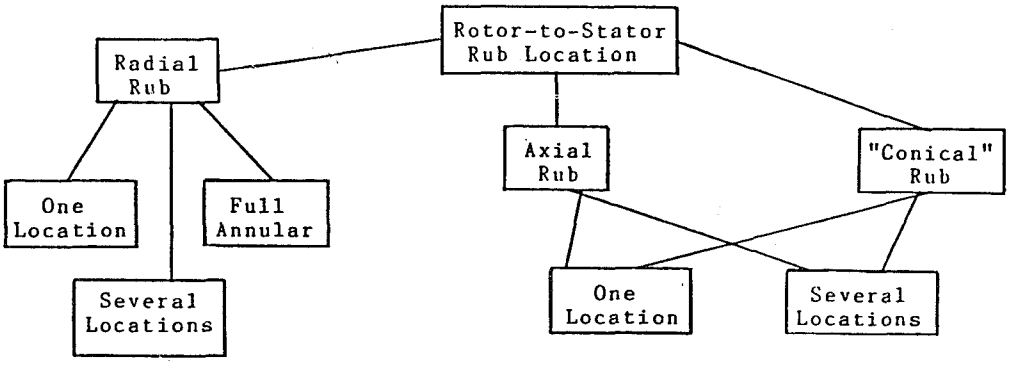

Figure 2. – Rotor–to–stationary element rub location.

$D_\nu \tilde{z}_\nu/\kappa_\nu$. The coefficients f_ν describe the timing of "contact" (f_ν=1 for $|\tilde{z}_\nu| \geq C_\nu$) versus "no contact" ($f_\nu$=0 for $|\tilde{z}_\nu| < C_\nu$). The functions $K_{r\nu}(|\tilde{z}_\nu| - C_\nu)$ describe the radially applied additional stiffness force due to contact with the stationary part. They also describe the rotor/stator normal forces. The functions $K_{r\nu}(|\tilde{z}_\nu| - C_\nu)j\mu_\nu$ model the tangentially oriented friction forces. The coefficients κ_ν describe an additional energy loss due to local material

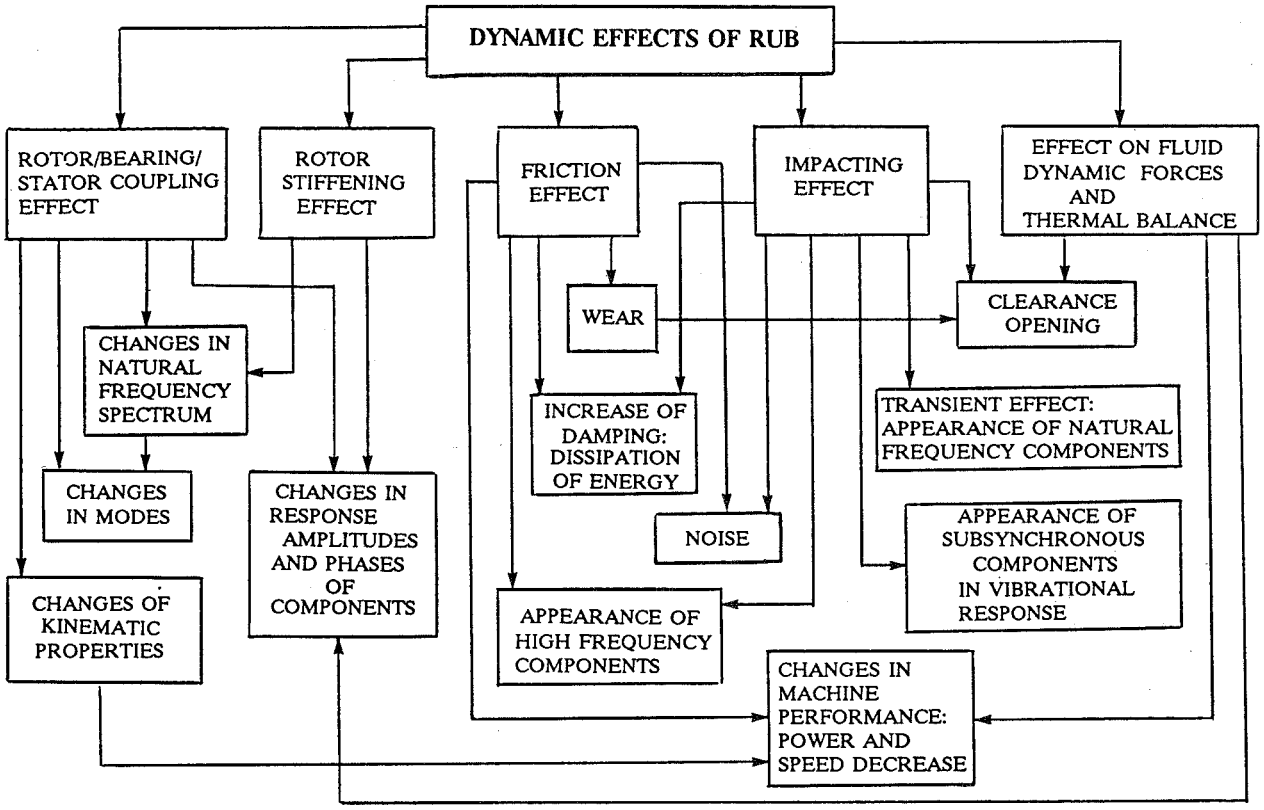

Figure 3. – Dynamic effects of rotor–to–stationary element rubbing.

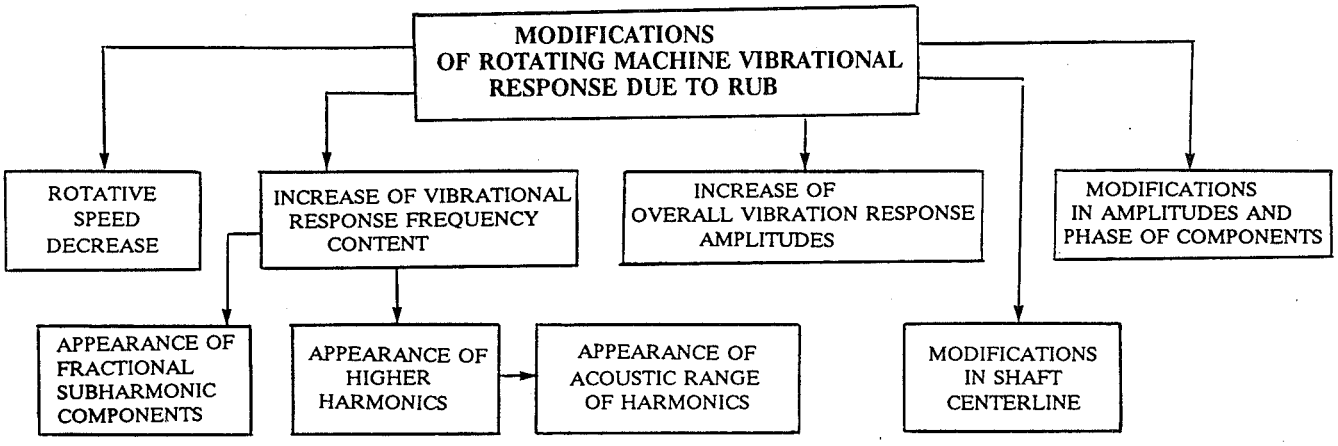

Figure 4. - Modifications of rotating machine vibrational response due to rotor-to-stationary element rubbing.

deformation during the impacting condition. The definition of κ_ν, as explained below, differs, however, from the classical restitution coefficient definition.

Before the rotor–to–stator contact occurs, for example, at the first seal, i.e., for $|\tilde{z}_1| - C_1 < 0$ there is $f_1 = 0$ and $\kappa_1 = 1$, thus, from Eq. (2) for ν=1:

$$D_1(\dot{\tilde{z}}_{1(-)} - j\lambda_1\Omega\tilde{z}_1) + (K_{B1} + K_1)\tilde{z}_1 - K_1 z_1 = 0\ , \tag{3}$$

where the velocity subscript $_{(-)}$ indicates the "before collision" situation. Following the classical impact theory, during collision only velocities are instantaneously affected. Displacements remain the same. Just after collision, i.e., for $|\tilde{z}_1| - C_1 \geq 0$ there is $f_1 = 1$ and $\kappa_1 < 1$, thus

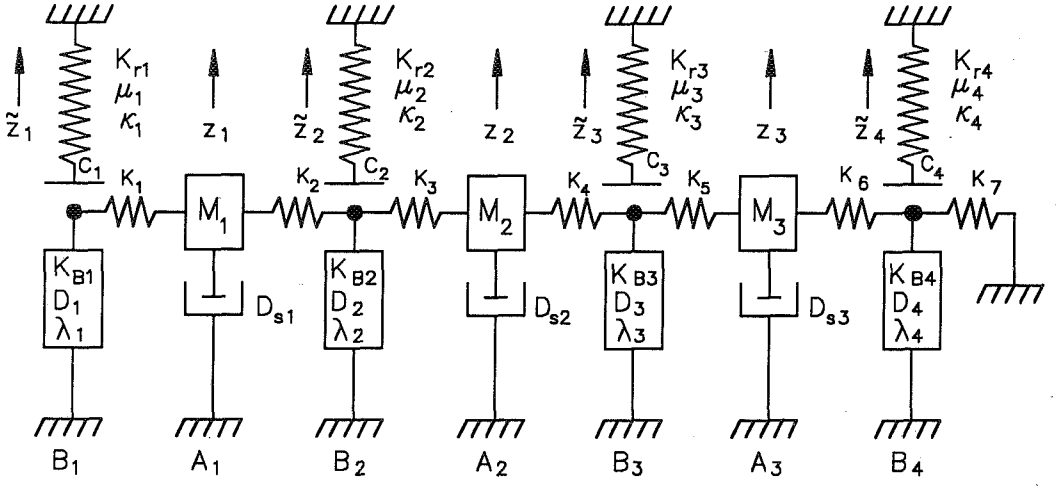

Figure 5. – Rotor system model.

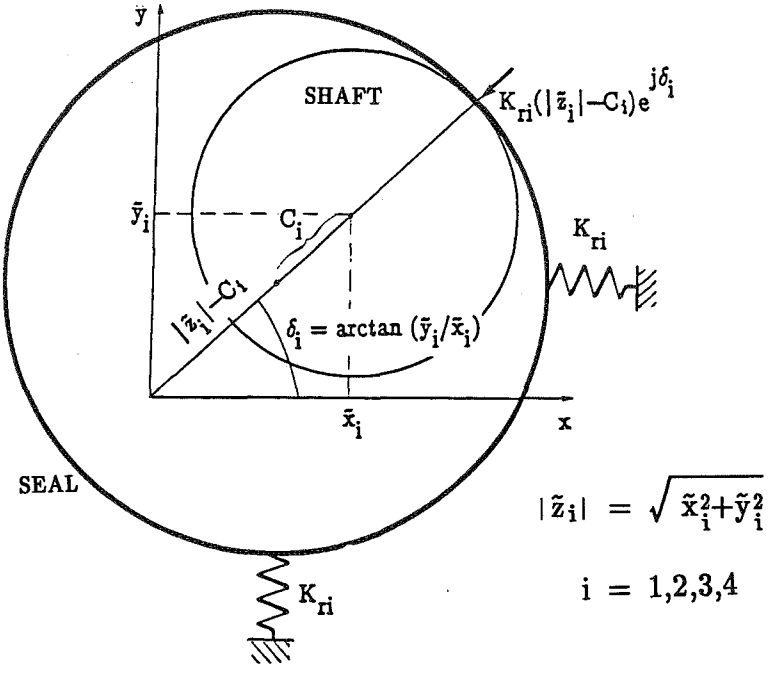

Figure 6. – Rubbing rotor inside a seal.

$$D_1(\dot{\tilde{z}}_{1(+)}/\kappa_1 - j\lambda_1\Omega\tilde{z}_1) + (K_{B1}+K_1)\tilde{z}_1 - K_1 z_1 + K_{r1}(|\tilde{z}_1| - C_1)(1+j\mu_1)e^{j\delta_1} = 0 \,, \tag{4}$$

where the velocity subscript $_{(+)}$ indicates the "after collision" situation. Taking into account Eqs. (3) and (4) the coefficient of restitution κ_1 is defined as follows:

$$\kappa_1 = \frac{\dot{\tilde{z}}_{1(+)}}{\dot{\tilde{z}}_{1(-)} - K_{r1}(|\tilde{z}_1| - C_1)(1 + j\mu_1)e^{j\delta_1}/D_1} \tag{5}$$

Note the differences in this definition, as compared to the classical straight impact theory. In Eq. (5) both velocities $\dot{\tilde{z}}_{1(-)}$ and $\dot{\tilde{z}}_{1(+)}$ have the same sign. There is no justification to assume that in the rotor lateral planar motion the impact against a compliant stator causes velocities to reverse immediately. The second difference is the addition of the stator stiffness–related normal and tangential forces, modifying the "after collision" velocity. When the stator stiffness is low the after collision motion continues in the same direction until, due to an increase of displacement $\tilde{z}_1$, a balance occurs, and $\dot{\tilde{z}}_{1(+)} = 0$. At this moment the motion is reversed. The similar impact situations take place at all possible rub locations ν=1,2,3,4.

ROTOR–TO–STATOR RUB COMPUTER SIMULATION PROGRAM

The computer program was written to help explore the effects of rotor–to–stator rub on rotor vibrational responses.

The computer program is composed of two major subprograms: (1) the linear rotor/bearing/seal system synchronous response with no rub, and (2) the timebase response of the nonlinear system with rub at a selected constant rotative speed. The first of the subprograms allows the user to calculate the static displacement and synchronous (1×) response of the system versus rotative speed, producing transient type data which may be displayed in Bodé or polar plot format. This allows for easy identification of the system three–mode modal characteristics and resonances, indicating at which rotative speeds the largest vibration amplitudes occur. This information is used to determine rotative speed ranges which should be investigated more closely by taking into account the rub effects in the timebase response. The second portion of the program allows a more detailed analysis of the shaft vibrational response caused by external and rub–related exciting forces at the desired rotative speeds, by calculating (using numerical integration) the shaft centerline motion versus time. In addition to the linear parameters of the shaft and support structure, the timebase response subprogram uses the nonlinear properties of the rotating system imposed by outside support structures with limited clearances.

The overall program sequence is shown using the flow chart in Figure 7. The program computes data buffers for both the linear and nonlinear responses at each of the three mass stations, A_i, and each of the four bearing/seal locations, B_ν (Fig. 5), plus buffers indicating positions and time periods of rotor–to–stator contacts. The parameters necessary to allow computation of the synchronous response include the following: the system modal mass at each mass station, the stiffness for each shaft section, the external damping at each mass location, the rotational unbalance force vector, the radial constant preload force and its associated angle, and the fluid radial damping, fluid average circumferential velocity ratio, fluid radial stiffness, and radial clearance at each of the bearing/seal locations.

After the system parameters have been entered and verified, the program begins the execution of the synchronous response calculations. If the synchronous vibration response is not

required, the program skips the calculation and proceeds to the nonlinear calculations described below. Otherwise, the program prompts for the rotative speed range and increment between calculations over which the synchronous calculations are to be performed. Once this data has been entered, the program proceeds to calculate the synchronous response of the rotor at axial locations $A_1,...,A_3$ (disk locations) and $B_1,...,B_4$ (bearing/seal locations). The program solves the linear portion of the equation set (for $\kappa_\nu=1$ and $f_\nu=0$) by assuming solutions of the following form:

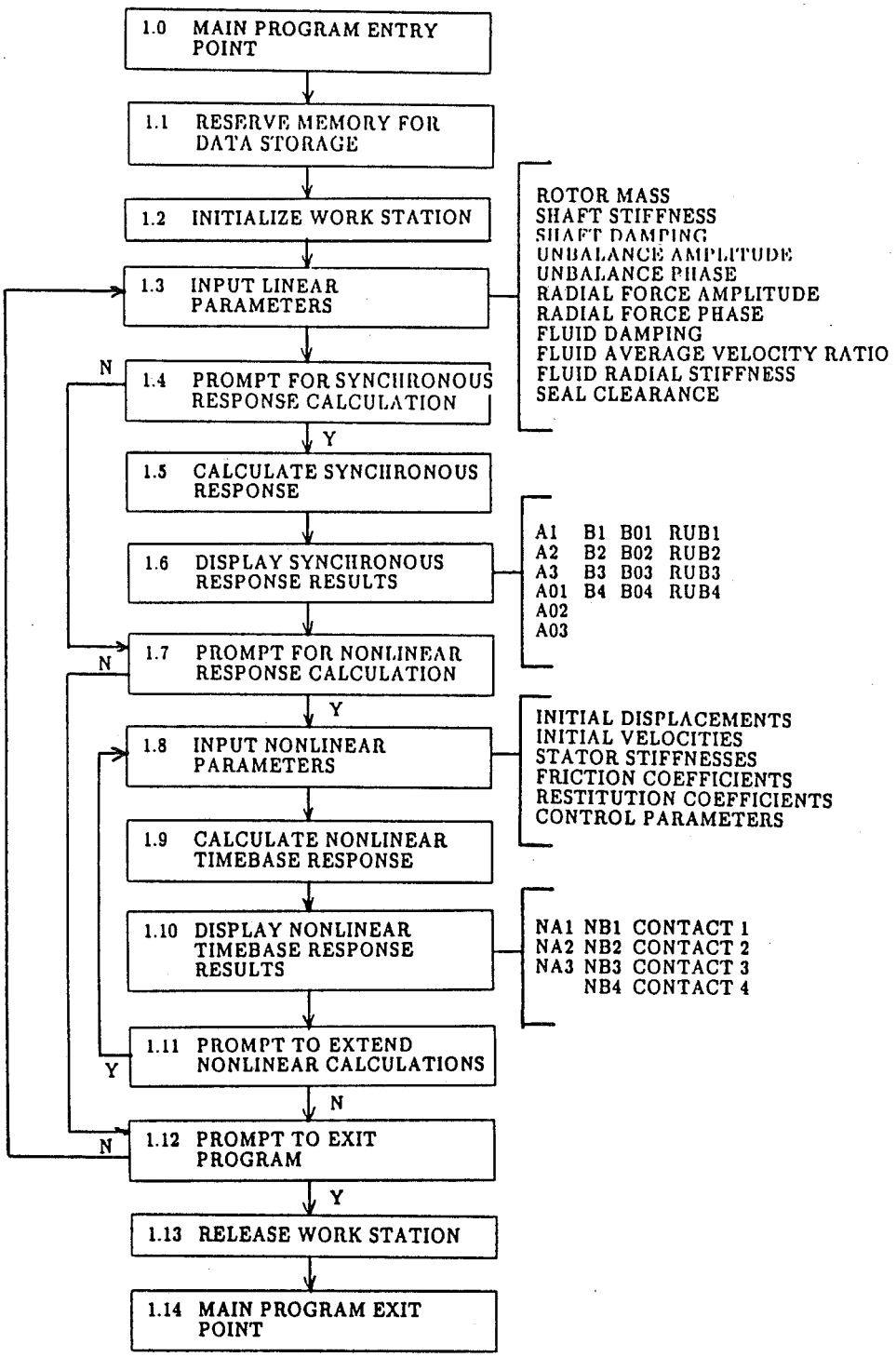

Figure 7. – Flow chart of main program sequence.

$$z_i = A_i e^{j(\Omega t + \alpha_i)} \quad \text{and} \quad \tilde{z}_\nu = B_\nu e^{j(\Omega t + \beta_\nu)}$$

for the unbalance force response, and

$$z_i = A_{oi} e^{j\alpha_{oi}} \quad \text{and} \quad \tilde{z}_\nu = B_{o\nu} e^{j\beta_{o\nu}}$$

for the static radial preload force response. These solutions are then substituted into the original equations (1) and (2), which are eventually solved to get the amplitudes and phases of the response at each location. The maximum amplitude and its angle is calculated for each bearing/seal location by combining the unbalance and preload responses for that location. These values are then compared with the specified radial clearance at the location to determine whether rubs would have occurred. This information is placed in the "RUB" data buffers, which may be displayed in the same manner as the vibration responses. The linear system response data, and potential rub information may be plotted using a Bodé format or listed in tabular format either on the computer screen or a graphics printer.

If the nonlinear calculations are not required, they may be skipped, and the program proceeds to the exit. If they are to be performed, the additional parameters necessary to complete the calculations must be entered. These include the initial displacements and velocities at each location (initial conditions), the stator stiffness, the coefficient of friction at the rotor and stator surfaces, and the impact restitution coefficient at each of the potential rub locations, plus the program control variables, namely operating speed, number of revolutions to compute, and the number of computational steps per revolution.

If the linear calculations by the first portion of the program were performed, the initial displacements and velocities are calculated from the synchronous responses; therefore, any values entered during the data input process will not be used by the program. The initial conditions in the parameter table are also not used when the nonlinear calculations are being extended. The process of extending the nonlinear calculations is discussed later; for now it is sufficient to realize that the initial conditions for the current calculation are obtained from the previous calculation, and their input into the parameter table is not required.

Instead of assuming a solution form and substituting it into the original equations as was done to get the linear solution, the numerical integration algorithm requires that each equation be solved for its highest order derivative. The Runge–Kutta algorithm then uses the values calculated for the highest order derivatives, along with the current state of the system, (shaft positions and velocities) to predict the state of the system at some point in the future. This process continues until the motion for the specified period has been calculated. The accuracy and numerical stability of the algorithm is very sensitive to the step size between computed points. Large step sizes provide increased computational speed at the cost of reduced accuracy and stability, since both accuracy and stability depend on the product of the step size and the value of the highest order derivative. This program uses a variable step size, based on the percentage change between the value for the new point and the current point, to optimize both the computational speed and accuracy. Figure 8 illustrates this process by showing the steps for a possible computation sequence between two data sample times. Since any change from the value of zero will produce percentage changes greater than allowed, the program also has an amplitude threshold which overrides the change requirements between points if the new value is less than the threshold. The threshold and percent change parameters should be picked carefully as they significantly affect both the computational speed and accuracy.

Once the computations are performed and data buffers have been completed, the nonlinear motion may be displayed using an orbit/timebase format or numerically listed.

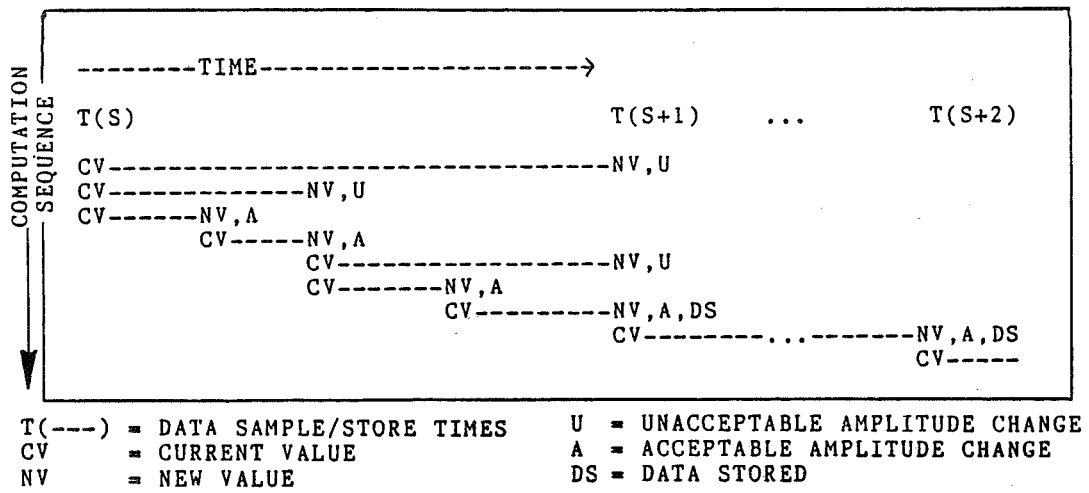

Figure 8. – Computational sequence for variable step size Runge–Kutta numerical algorithm.

The program allows the nonlinear calculations to be extended. The extension can be used to continue the computational period until a steady–state solution is obtained by using the values at the last computed point as the initial conditions for another computational period. This process can be continued until the steady–state solution has been obtained. The computational results are discussed later in this paper.

ROTOR–TO–STATOR RUB EXPERIMENTAL RIG

A series of tests involving partial rotor–to–stator rub were performed on a two lateral–mode rotor rig. The rotor/stator contact was carefully documented and correlated with the rotor vibrational responses.

The rotor rig (Figs. 9 and 10) consists of a horizontal isotropic two–disk rotor supported at each end by a relatively rigid bronze sleeve–type bearing (Oilite). A 0.5 horsepower ac motor drives the rotor through a flexible coupling. When observed from the motor end of the shaft (inboard end), rotation is in the counterclockwise direction. Horizontal brass screws are mounted adjacent to each of the two rotor disks, both at angle 270°. The rub screws, when used in conjunction with the rotor, allow engaging the rotor in the partial rotor–to–stator rub conditions. Of particular interest in this experiment is the influence of multiple axial locations of partial rub on rotor dynamic response, i.e., rub occurring simultaneously at more than one plane along the machine train.

The XY displacement probes providing the shaft radial displacement data are mounted next to each rotor mass. A Keyphasor® probe mounted vertically at the inboard end provides the once–per–turn reference signal from which all phase angles are measured in the direction against rotation. The shaft observing vertical and horizontal probes are installed at 0 and 270 degrees respectively.

Located at the rotor midspan is a shaft preloading fixture. The fixture consists of a small ball bearing mounted on the shaft and radially supported by four orthogonal springs. Each spring of stiffness 16 lb/in is attached to the stationary fixture frame.

An extremely "light" rub may not be apparent through vibration signals. Shaft vibration data is, therefore, correlated with a rub contact timing signal in a timebase format. This timing signal accurately identifies a rotor–to–stator contact condition. A 1–volt–dc potential is placed

A – ELECTRIC MOTOR
B – FLEXIBLE COUPLING
C – INBOARD BRONZE BEARING
D – ELECTRICAL CONTACT DEVICE
E – INBOARD X Y DISPLACEMENT PROBE MOUNT
F – INBOARD MASS
G – INBOARD HORIZONTAL RUB SCREW
H – X Y PRELOAD FIXTURE
I – OUTBOARD HORIZONTAL RUB SCREW
J – OUTBOARD MASS
K – OUTBOARD X Y DISPLACEMENT PROBE MOUNT
L – OUTBOARD BRONZE BEARING
M – ROTOR SHAFT
N – ROTOR BASE

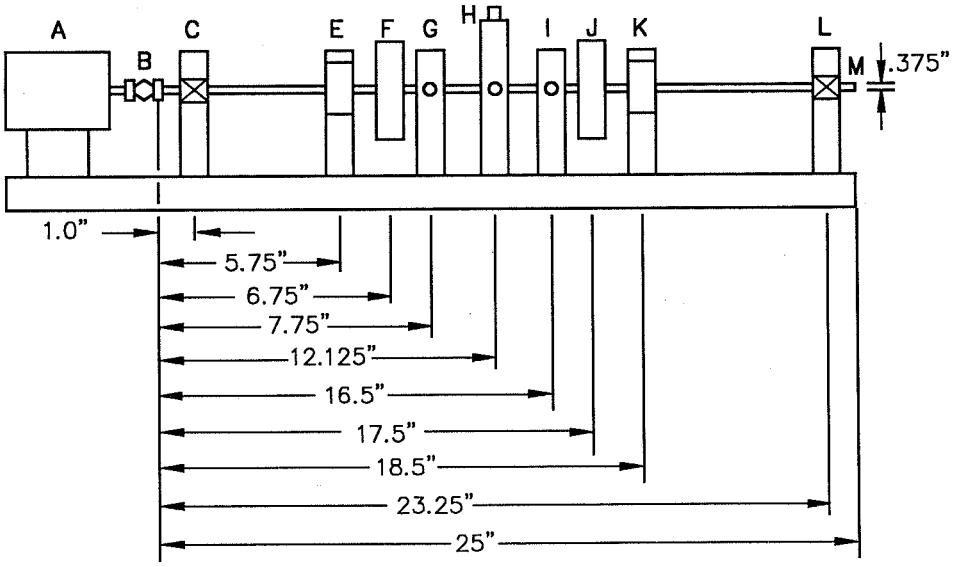

Figure 9. – Experimental rig.

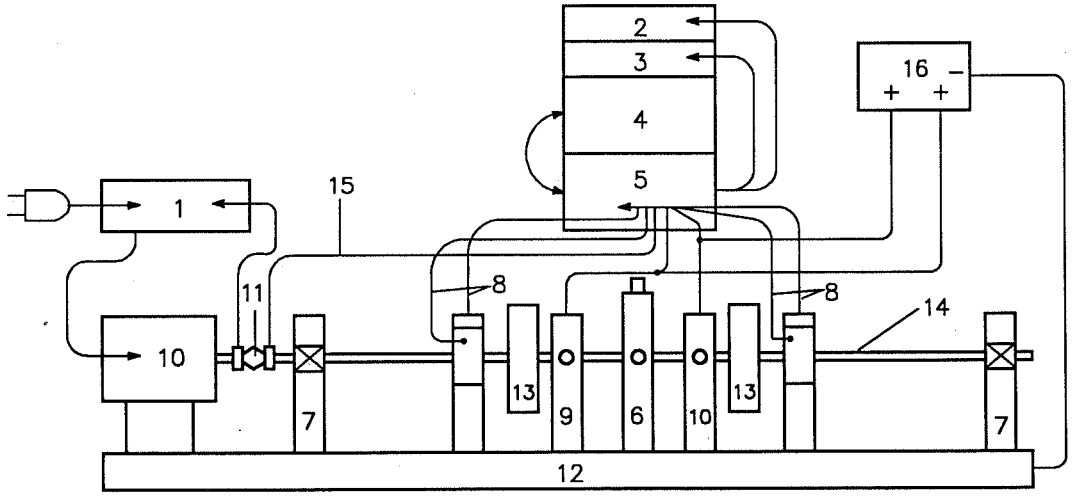

1. MOTOR SPEED CONTROL
2. TRACKING FILTER
3. SPECTRUM ANALYZER
4. COMPUTER
5. 108 DAI
6. X Y PRELOAD FIXTURE
7. BRONZE BEARINGS
8. X Y EDDY CURRENT DISPLACEMENT PROBES
9. INBOARD HORIZONTAL RUB SCREW
10. OUTBOARD HORIZONTAL RUB SCREW
11. FLEXIBLE COUPLING
12. ROTOR BASE
13. 3 INCH DIAMETER DISCS
14. ROTOR SHAFT
15. KEYPHASOR PROBE
16. dc DUAL POWER SUPPLY
17. ELECTRIC MOTOR

Figure 10. – Experimental Data acquisition system.

across the rotor and an electrically isolated rub screw. The mechanical/electrical contact between the rotor shaft and each rub screw provides a circuit yielding continuity position/timing data correlated to both the Keyphasor and vibration signals.

The vibration information from the proximity probes is presented in shaft orbit and timebase formats, and eventually processed through filters and an FFT analyzer to determine the frequency components contributing to the overall waveform. The information on lateral vibration from different axial locations of the shaft can then be correlated to provide rotor deflection shape.

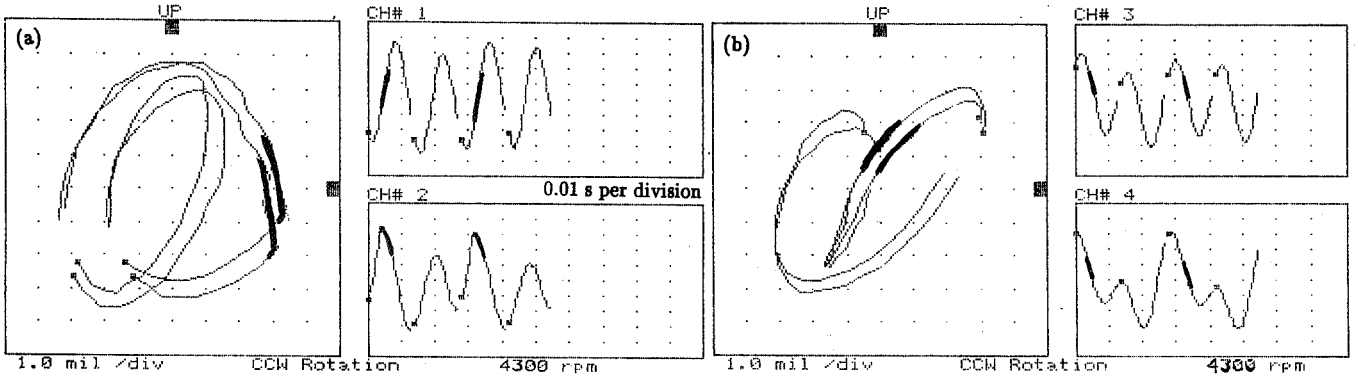

Figure 11. - Rubbing rotor inboard (a) and outboard (b) responses at a constant rotative speed 4300 rpm. Rubbing timing is marked using thick lines.

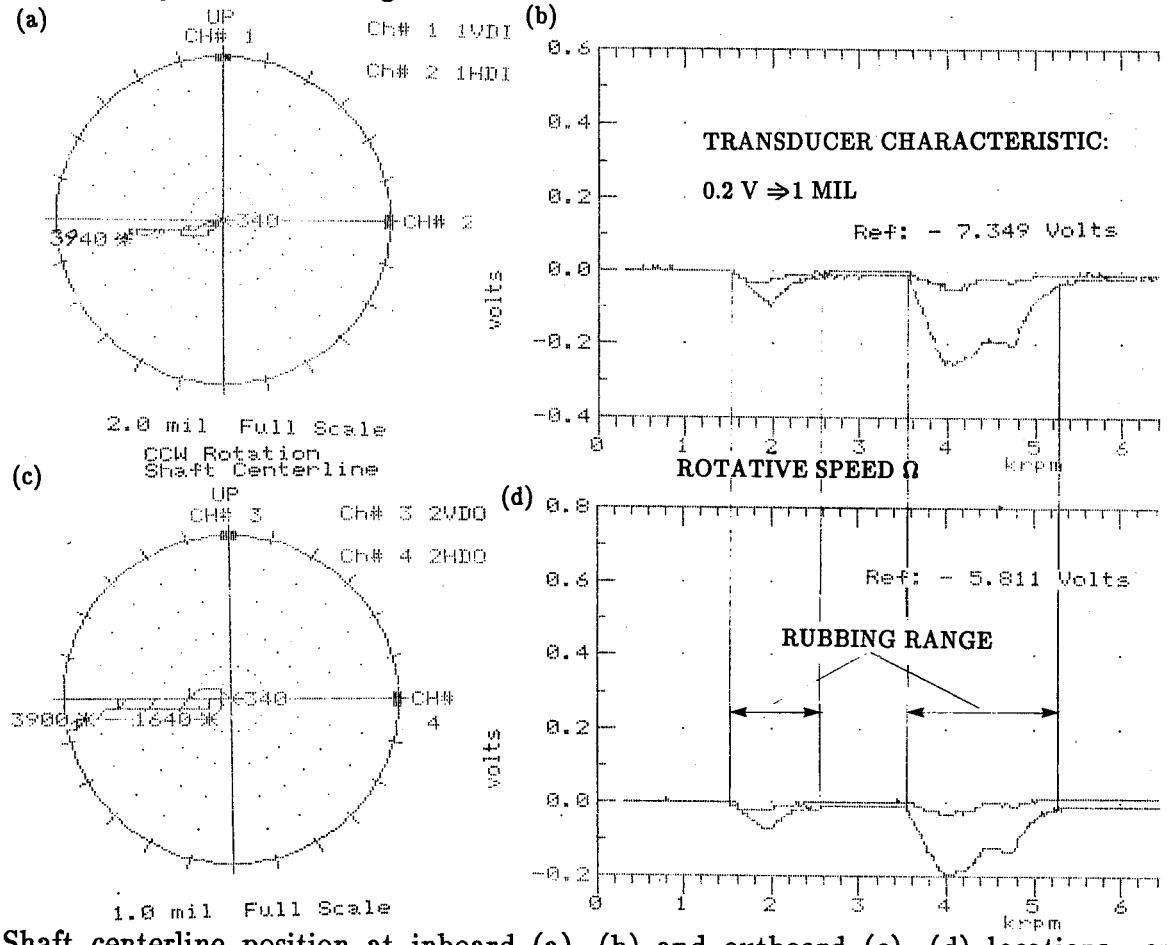

Figure 12. - Shaft centerline position at inboard (a), (b) and outboard (c), (d) locations versus rotative speed in the polar and orthogonal formats. Note significant displacements in the horizontal direction at speeds when rub occurs.

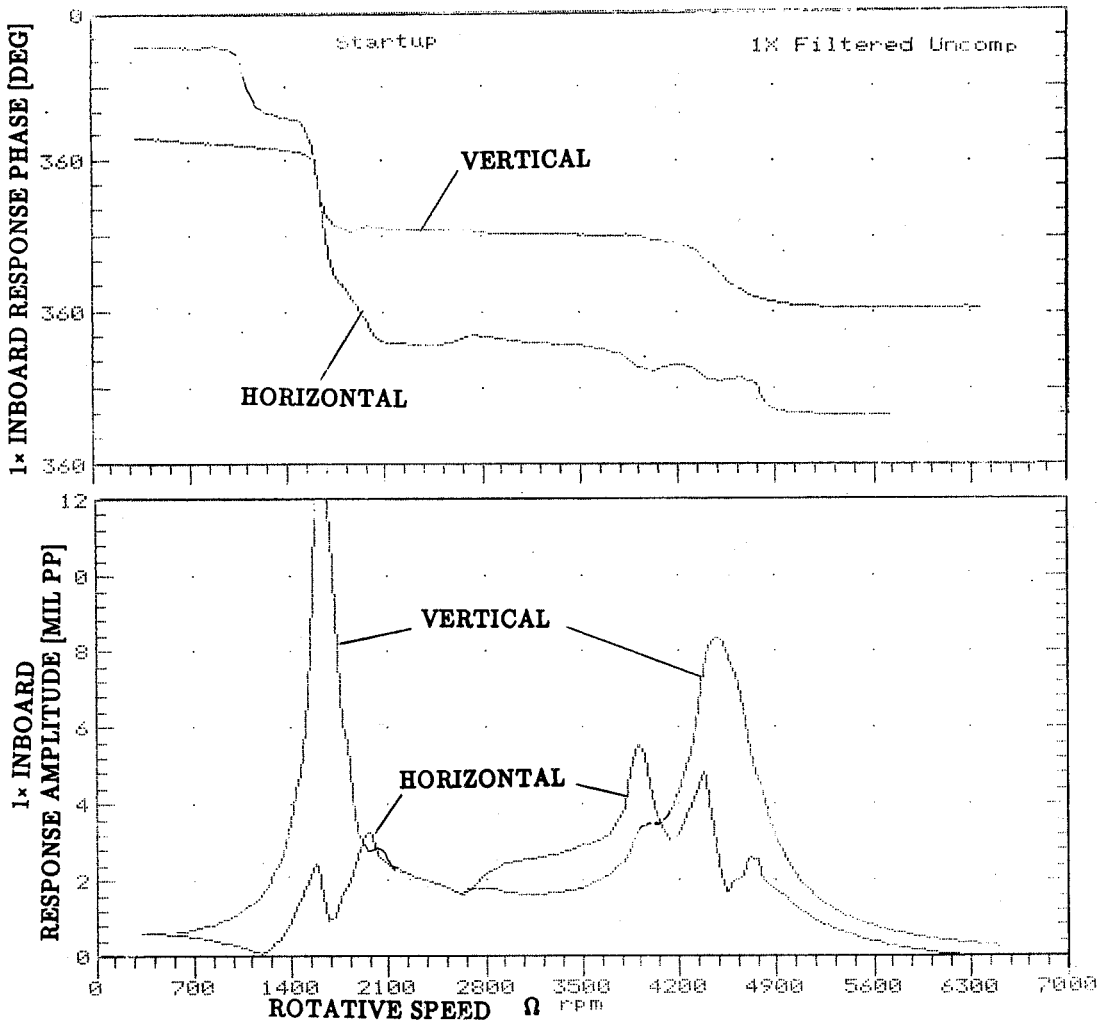

Figure 13. - Bodé plot of rubbing rotor 1× inboard vertical and horizontal responses. Note significant changes in the horizontal response, the direction where the main rubbing activity occurs.

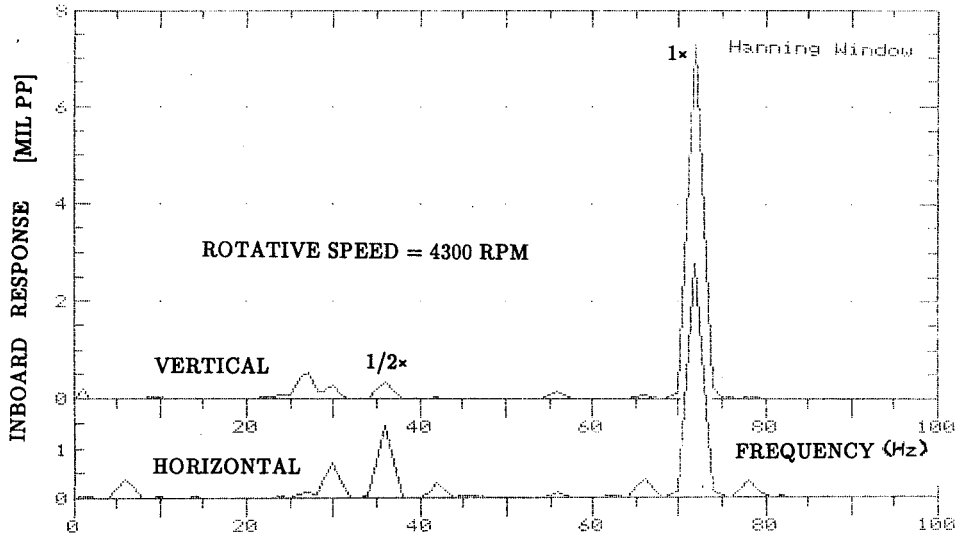

Figure 14. – Rubbing rotor vibration spectrum at 4300 rpm.

TEST PROCEDURE AND TRANSIENT TEST DATA

A controlled unbalance inserted at the rotor inboard disk is used to generate the required level of synchronous vibration for the rub initiation. Rotor speeds range from 0 to 6500 rpm passing through the rotor first and second balance resonances at approximately 1580 rpm and 4200 rpm respectively. It should be noted that these speeds represent the rotor's first and second balance resonances under normal operating conditions without rub.

The unbalance mass employed for this series of experiments is 0.5 grams at a radius of 30.5mm at 0 degrees (relative to the Keyphasor notch). Each rubbing rotor data run was initiated by locating the appropriate brass rub screw close to the rotor shaft. A light horizontal preload (1 to 2 lb) was then introduced at the rotor midspan.

EXPERIMENTAL RESULTS: RUB WITH PREDOMINANT SECOND MODE 1× VIBRATION

Past experimentation [2–4,6] has focused on the rules for single point rubs occurring in rotating shafts operating in the range of predominantly first lateral mode 1× vibrations of the rotor. Vibrations were observed at the shaft axial location where the rub occurred. The rotor rig used in the present experiments allows examination of the shaft vibration pattern at several axial locations. The first two natural frequencies of the system are close enough that they fall in the range of investigated rotative speeds. The corresponding modes are bending modes of the shaft. When more than just one mode can be involved, the interpretation of the rub–related vibrations and identification of rub radial location must be done more carefully. An example is given in Figs. 11 to 15. Figure 11 presents inboard and outboard shaft vibration time base waveforms and orbits during rubbing at a constant rotative speed 4300 rpm, higher than twice first balance resonance frequency, and slightly lower than the second balance resonance frequency of the rotor. The operating speed falls into the range of the second mode, thus the basic 1× vibrations at the inboard and outboard locations are out of phase. By using information from the rotor–to–stator physical contact device, the identification of the rubbing location was not difficult: rubs occur on the inboard side at 270° where the screw is mounted. If, however, only outboard vibration data were available, the rub location might be erroneously identified on the opposite side (outboard, and at 90°).

Figure 12 presents important data which is often overlooked, namely, the shaft centerline position. When the rub occurs, the shaft is rebounding away from the contact point. Figure 13 presents the Bodé plot of the rubbing rotor synchronous (1×) response indicating significant changes in the horizontal component. The spectrum contents at 4300 rpm is given in Figure 14. Two Keyphasor dots at the orbits (Fig. 11) confirm the appearance of the 0.5× component in the rotor response. Figure 15 illustrates the rubbing shaft centerline changes.

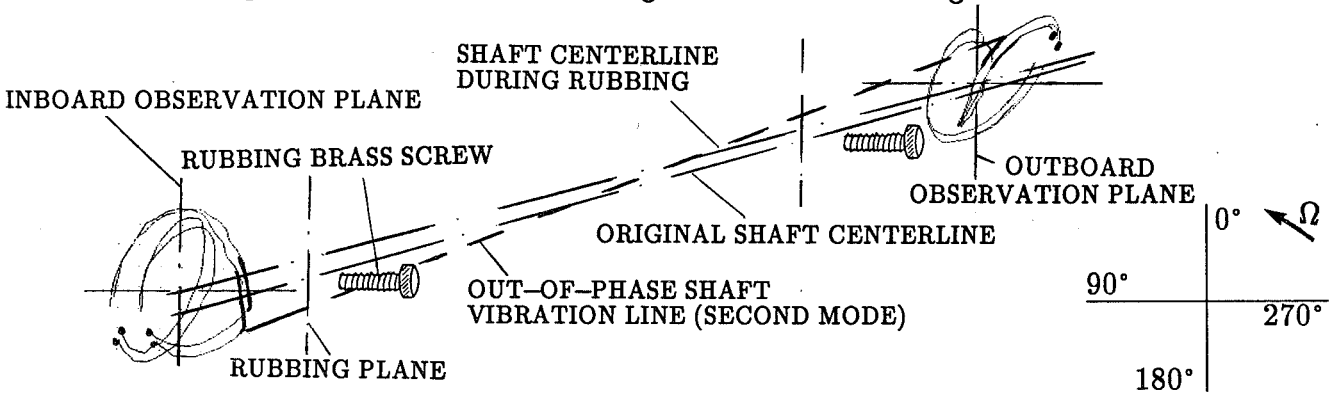

Figure 15. – Rubbing rotor centerline at 4300 rpm.

EXPERIMENTAL AND ANALYTICAL RESULTS FOR RUBBING ROTOR AT CONSTANT ROTATIVE SPEEDS

The figures 16 to 19 illustrate the corresponding experimental and analytical results. The data in Figures 16a through 19a are the orbit/timebase waves at various operating speeds produced by the experimental rotor rig during a routine start–up. The synchronous force was generated by placing a mass unbalance in the outboard disk. The rub boundary was established by adjusting the brass rub screw next to the inboard disk until it was close to the shaft. Using the bias springs, the shaft was then preloaded toward the rub boundary enough to cause contact as the rotor synchronous vibrations increased in resonant ranges of rotative speeds. Figures 16a and 17a are the vibrational responses at a constant speed near the first balance resonance frequency, while Figures 18a and 19a are the responses near the second balance resonance frequency. Figures 16b through 19b are the simulated vibrational responses generated by the computer program for the same conditions, as the associated experimental responses. If one waveform is taken as an example, illustrated figures a and b respectively, the experimental and computer–generated responses, can be compared. The timebase waveforms in the horizontal direction where the rub occurs are almost identical. The instances of contact, indicated by the highlighted portion of the waveforms, occur at the same locations for both responses, and also have approximately the same duration. The largest difference in these two response waveforms is

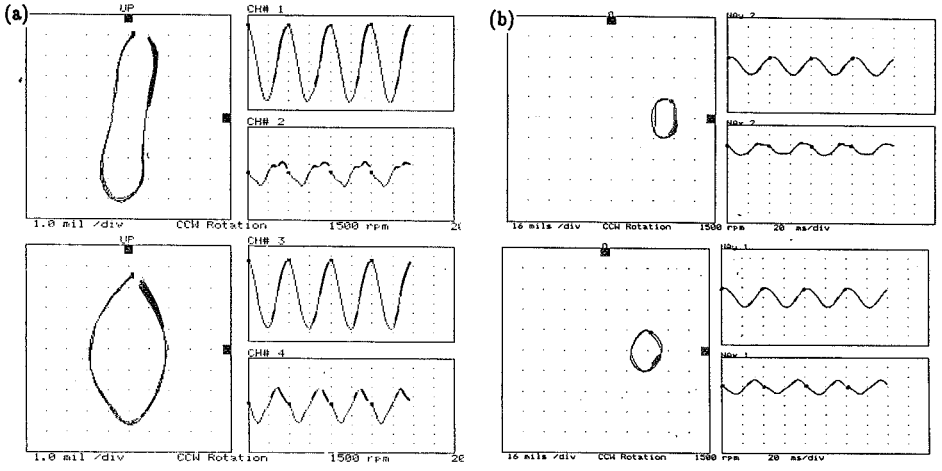

Figure 16. - Rubbing rotor inboard and outboard orbits and waveforms at 1500 rpm: (a) experimental, (b) computer-simulated.

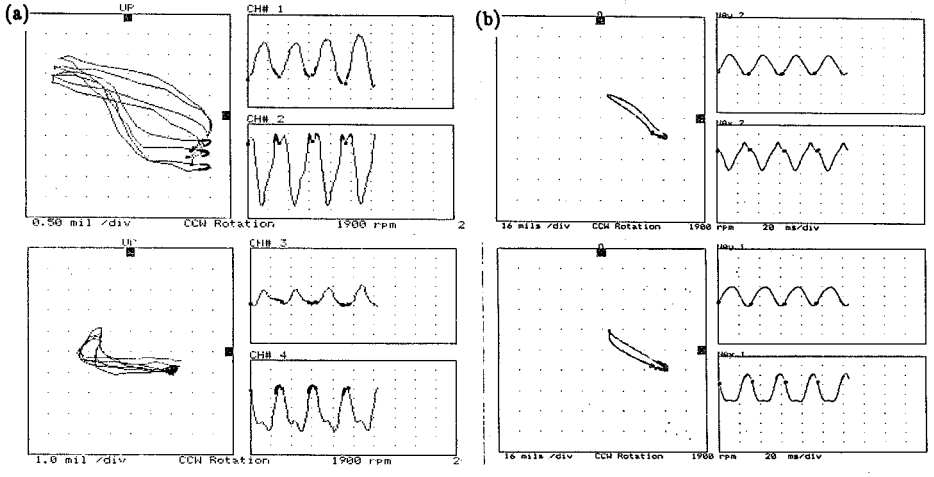

Figure 17. - Rubbing rotor inboard and outboard orbits and waveforms at 1900 rpm: (a) experimental, (b) computer-simulated.

TABLE 1

M_1=0.005 lb s^2/in
M_2=M_3=0.0025 lb s^2/in
K_1=K_6=182 lb/in
K_2=K_4=K_5=10^4 lb/in
K_{ri}=10^4 lb/in
K_3=460 lb/in
D_{si}=0.03 lb s/in
F_{u1}=$2.5 \cdot 10^{-5}\Omega^2$ lb
F_{u2}=F_{u3}=0
ε_1=90°
F_{p1}=F_{p2}=0
F_{p3}=9 lb
γ_3=0°
D_1=D_4=0.1 lb s/in
D_2=D_3=0.01 lb s/in
λ_i=0
K_{B1}=K_{B4}=900 lb/in
K_{B2}=K_{B3}=0
C_1=C_2=C_4=10 in
C_3=0.05 in
μ_i=0.5
κ_i=1 i = 1,2,3,4

the ratio of the forced vibration magnitude to the transient vibration caused by the rubbing forces. The vertical experimental and analytical response waveforms also show similar patterns. The major difference between the experimental and computed responses is related to the phases between the horizontal and vertical responses. In the experimental responses the maximum negative vertical excursion occurs at about the same time as the maximum negative excursion of the horizontal response. For the computed responses the maximum negative vertical excursion occurs when the horizontal response reaches maximum positive. This timing difference is caused by the relationship between the forced vertical response and the transient vertical response. Since the orbit format is very sensitive to the relative phases between the orthogonal waveforms, it shows the greatest difference between experimental and computed responses. Relatively large numbers of inter–related variables controlling the response and the long computational time period required to reach a steady–state solution results in an approximation to the corresponding experimental data. The two–mode rotor system modal parameters were identified prior to rubbing occurrences [5]. The identification of rub–related parameters was more difficult, and some estimation was applied (Table 1). This certainly contributes to the differences observed in the experimental versus analytical results. However, the main contributor to the differences is how the rub boundary is produced (see Figure 20). The experimental rub boundary is a flat vertical surface bounded in only one direction. The rub boundary used by the computer program is a full 360–degree circular clearance. To approximate the flat surface bounded only on one side, the computer program must use small unbalance forces combined with high preload forces and a

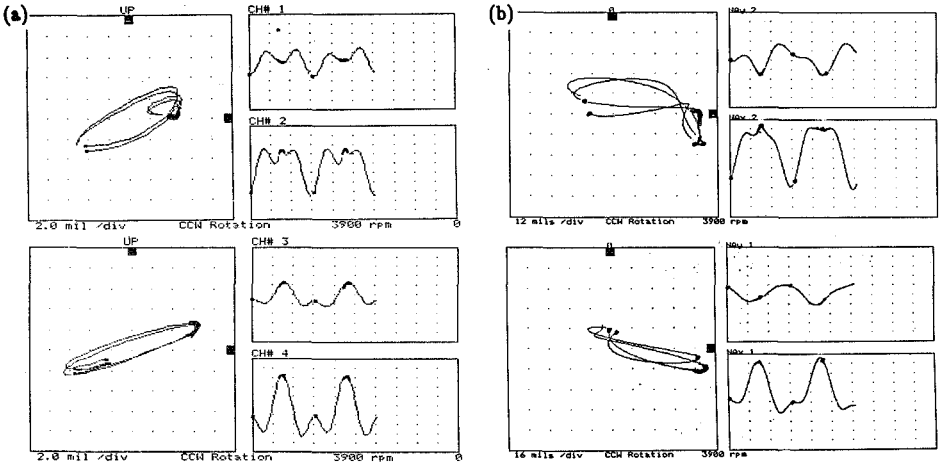

Figure 18. - Rubbing rotor inboard and outboard orbits and waveforms at 3900 rpm: (a) experimental results, (b) computer-simulated results.

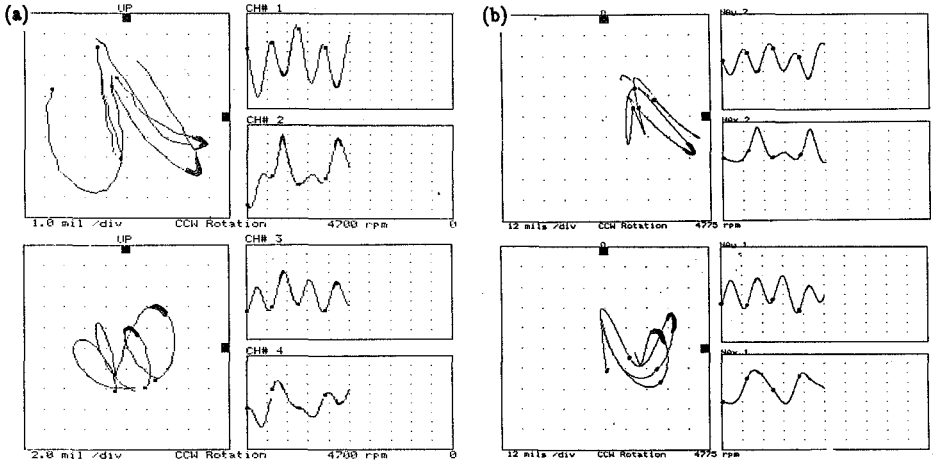

Figure 19. - Rubbing rotor inboard and outboard orbits and waveforms at 4700 rpm: (a) experimental results, (b) computer-simulated results.

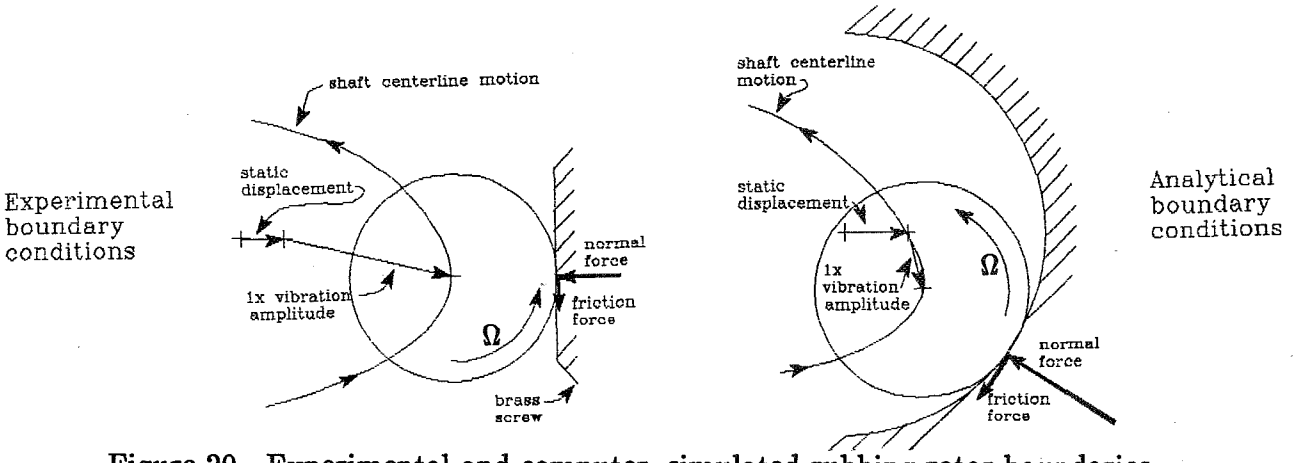

Figure 20.–Experimental and computer–simulated rubbing rotor boundaries.

relatively high clearance (Figure 6). The rotor centerline is moved away from the center of the clearance enough to allow the rebounding motion to occur within the available clearance. This process imposes limits on the ratio of unbalance to preload force. Since the impact force producing the transient motion depends on the combination of preload and unbalance forces, the unbalance response becomes a smaller part of the overall vibration. This explains the discrepancy in the ratio of forced–to–transient vibration amplitudes between the experimental and computer–generated data observed previously. The discrepancy concerning the timing relationship between the transient and unbalance responses in the vertical direction is also caused by the rub boundary configuration. When the shaft contacts the rub screw vertical surface in the experiment, there are two force components, the impact force and the tangential friction force in the downward direction for counterclockwise rotation. For counterclockwise rotation, the shaft in the computer program touches the seal simulating boundary below the clearance centerline if the combined preload and unbalance responses are greater than the clearance. The difference between this case and the experimental one is that now the impact surface is no longer vertical. Therefore, the impact force has a horizontal component similar to the experimental component, but also carries a vertical component in the up direction. If this component is higher than the friction–generated vertical down component, the net vertical force acts upward instead of downward like the experimental case. This produces the timing difference in the vertical direction noted earlier.

RUBBING ROTOR AT TWO AXIAL LOCATIONS. ADDITIONAL OBSERVATIONS

The previous experimental data have resulted in characterization of the rub phenomena by means of shaft lateral vibration frequency content. There exists some general rules that have been widely accepted. Of interest in this case is the generation of subsynchronous vibration components tied to the rotor's running speed and the rotor first natural frequency. The generation of rub–related subsynchronous components in the order of $(1/2)\times$, $(1/3)\times$, etc., necessitated the rotor speed to be at least twice, three times, and so on, the rotor's first natural frequency. Further studies relating to this concept indicate that both the generation, as well as transitions between orders of subsynchronous components, is perhaps not as clear as once believed. These general rules are true in the case of the rotor–to–stator rub at a single point; however, multiple axial points of rub occurring simultaneously involve more complex rotor responses.

During setup and adjustment of the same rotor rig for the experiment with multiple axial rub points, the existence of subsynchronous components were observed at rotative speeds below twice the rotor first natural frequency. The frequency content of the spectrum and orbit stability at various running speeds below twice first natural frequency appeared to be highly sensitive to the severity of rub, as well as the amount of radial preload applied to the rotor.

Data is presented in Figures 21 and 22 to illustrate these phenomena. Response orbit/timebase waves of the rubbing rotor's measured at inboard and outboard planes clearly show the presence of (1/2)× vibrations, being most predominant in the horizontal direction.

The running speed of 3143 rpm is 157 rpm lower than twice the system's "unmodified" first natural frequency of 1650 rpm. (A "modification" of system resonance occurs due to the stiffening effects of rub, and typically raises the natural frequencies.) At this time, although not quantitatively resolved, the experimental results from multi–axial rubs support to a greater extent the presence of rub–generated subsynchronous (1/2)× components occurring at rotative speeds below twice first natural frequency. These experiments do not cover the range of rotative speeds much above twice first natural frequency, nor have more than two points of rub been investigated. These topics should be addressed during further research.

ADDITIONAL EXPERIMENTAL RESULTS OF THE MULTIPLE ROTOR–TO–STATOR RADIAL RUB CONTACTS AT ONE AXIAL LOCATION

The set of tests presented below illustrates results of multiple radial rotor-to-stator contacts at one axial location. A modified rub fixture is equipped with an electric contact device and a stationary rub block (Fig. 23). The half-cylinder area of possible rotor contact simulates a seal.

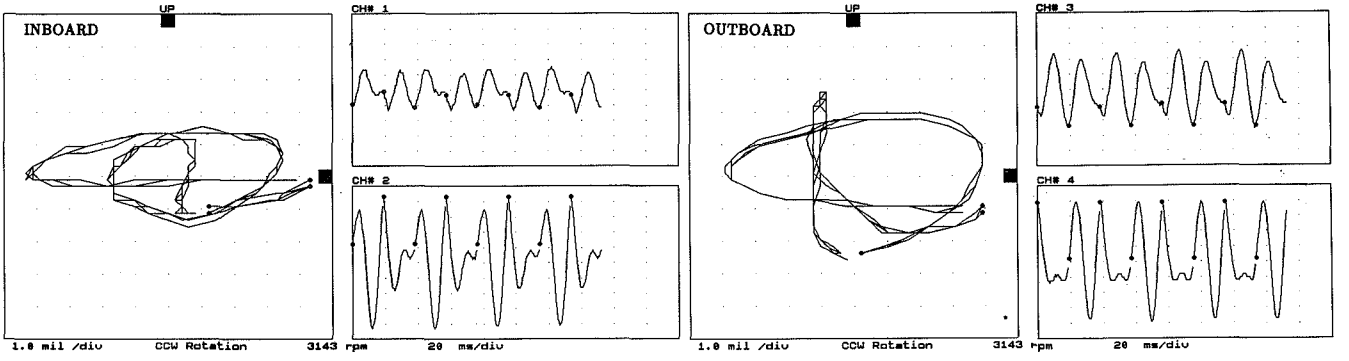

Figure 21. - Inboard and outboard rubbing rotor responses at the inboard and outboard locations at 3143 rpm. Orbits and timebase waves indicate presence of 1× plus (1/2)× components.

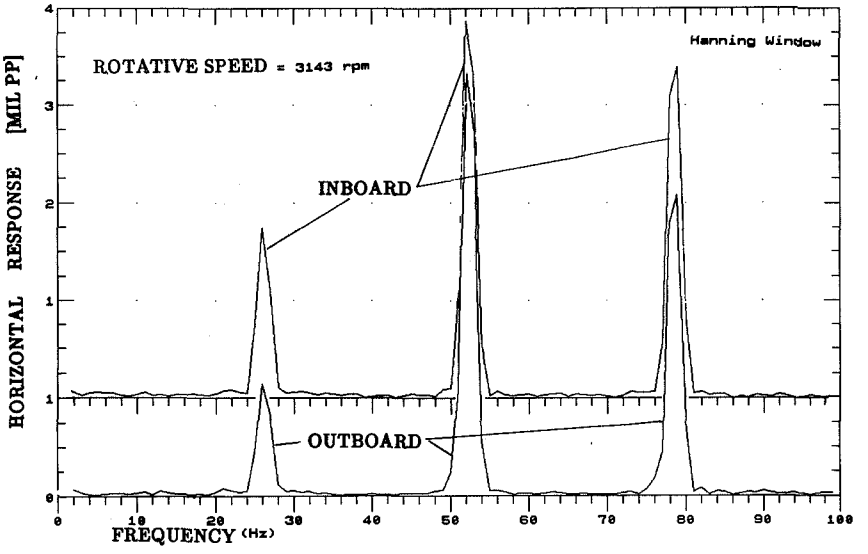

Figure 22. - Rubbing rotor vibration spectrum at 3143 rpm.

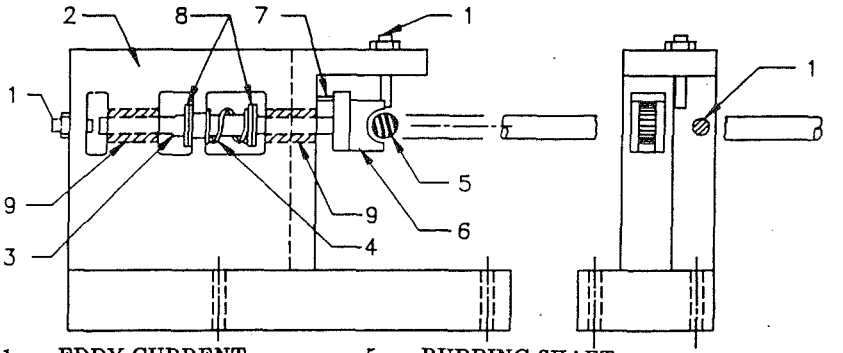

1. EDDY CURRENT DISPLACEMENT PROBE
2. FIXTURE BODY
3. PLUNGER SHAFT
4. COMPRESSION SPRING
5. RUBBING SHAFT
6. TEST RUB BLOCK
7. ALIGNMENT PIN
8. POSITION AND PRELOAD ADJUSTERS
9. LINEAR ANTI–FRICTION BEARING

Figure 23.–Semi–circular rub fixture.

Rub may practically occur at several radial positions. Most often it occurred at two locations. The rotor–to–stator contact information during rubbing at the first balance resonance speed range has been reduced in terms of "dwelling" time ratio and contact phase ratio versus rotative speed (Fig. 24). The "ratio" was obtained by relating the actual contact time to the period of 1× vibration at corresponding speeds. The 1× vertical response amplitude and phase are overlayed on the graphs. Note that the rotor–to–stator contact time ratio versus rotative speed resembles in shape the 1× amplitude, which suggests proportionality. Interesting is the contact phase, clearly following the 1× response phase lag.

FINAL REMARKS

This paper presents experimental and computer simulated results of rotor vibrational responses during multiple partial rubbing against a stationary elements. The considered cases are characterized by "light" rub conditions for which predominant in rotor responses are impacting/rebounding phenomena. The rotor/stator contact takes a small portion of the shaft rotational period so that the system stiffness increase effect is not high. The contact normal and friction forces are also relatively low. In continuation of previously studied rotor partial rub cases [2–6], this paper illustrates the rotor dynamic behavior when rubbing occurs at multiple axial locations of the shaft. It also emphasizes the importance of taking into account the shaft centerline position, as well as modal deflection line at specific rotative speeds for adequate identification of rotor–to–stator rub occurrences.

REFERENCES

1. Muszynska, A.: Rotor–to–Stationary Element Rub–Related Vibration Phenomena in Rotating Machinery, Literature Survey, The Shock and Vibration Digest, v. 21, No. 3, March 1989.

2. Muszynska, A., Bently, D. E., Franklin, W. D., Hayashida, R. D., Kingsley, L. M., and Curry, A. E.: Influence of Rubbing on Rotor Dynamics, NASA Contract No. NAS8–36719, Final Report, Bently Nevada Corporation, March 1989.

3. Muszynska, A.: Partial Lateral Rotor–to–Stator Rub, Third International Conference on Vibrations in Rotating Machinery, C281/84, IMechE, York UK, 1984.

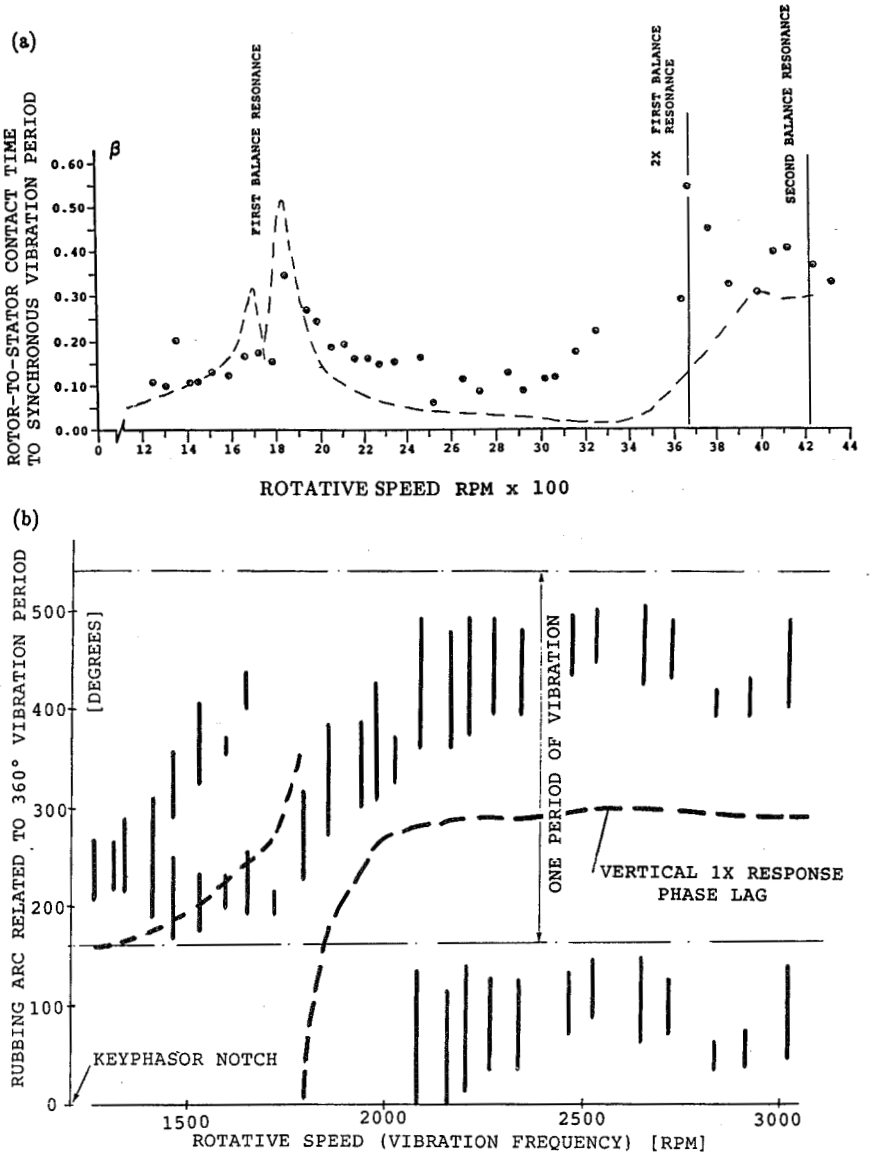

Figure 24. - (a) Rotor-to-stator contact in terms of the amount of shaft revolutions $\beta = \Omega t_c$ (t_c = contact time); (b) rub contact arc related to generalized vibration period versus rotative speed.

4. Muszynska, A.: Synchronous and Self–Excited Rotor Vibrations Caused by a Full Annular Rub, Eight Machinery Dynamics Seminar, NRC, Halifax N.S. Canada, 1984.

5. Muszynska, A., Bently, D. E., Franklin, W. D., and Hayashida, R. D.: Identification of Modal Parameters of Rotating Systems Using Perturbation Techniques, Part 1 and Part 2, Twelfth Biennial ASME Conference on Mechanical Vibration and Noise, Montreal, Canada, September 17–20, 1989.

6. Bently, D. E.: Forces Subrotative Speed Dynamic Action of Rotating Machinery, ASME Publication 74–DET–16, 1974.